Relativistic nonlinear dynamics of a driven constant-period oscillator

Seung-Woo Lee, Jung-Hoon Kim, and Hai-Woong Lee
Department of Physics, Korea Advanced Institute of Science and Technology, Taejon 305-701, Korea
(Received 4 April 1997)

The nonlinear dynamics of the constant-period oscillator (relativistic oscillator whose period is independent of energy) driven by a time-periodic external force is studied. It is shown that the oscillator displays nonlinear resonances and chaos when the driving force is sufficiently strong. Such nonlinear behavior arises from the fact that the frequency of the oscillator is shifted from its natural value and becomes energy dependent in the presence of an external force. Theoretical analysis of the resonances is given using the second-order canonical perturbation theory. [S1063-651X(97)10210-0]

PACS number(s): 05.45.+b, 03.30.+p

I. INTRODUCTION

Recently, we reported on fundamental mathematical and physical properties of a relativistic oscillator whose period is independent of energy, which we refer to as the constant-period oscillator (CPO) [1]. In this work we study classical dynamics of the CPO driven by a time-periodic force.

The CPO is a relativistic counterpart of the simple harmonic oscillator (SHO) in the sense that both SHO and CPO are characterized by an energy-independent period of motion. The period of the SHO is constant as long as one remains in the nonrelativistic regime, and this is essentially why the SHO, even when driven by a time-varying external force, is entirely free of chaos. As one enters the relativistic regime, however, the period of the SHO is no longer independent of energy, which gives rise to the generation of nonlinear resonances and eventually to chaos when a sufficiently strong external force is present [2]. It can then be immediately suggested that, when relativistic effects are taken into account, the system that is most resistant to the generation of nonlinear resonances and to chaotic behavior would be the CPO, a direct motivation for this study.

As reported in this paper, however, the driven CPO is not entirely free of chaos. Our numerical calculations show that nonlinear resonances are generated and, when these resonances overlap, chaotic behavior occurs. The origin for such chaotic behavior of the driven CPO lies in the fact that the period of the CPO is no longer constant in the presence of an external force. This is what differentiates the CPO from the SHO. The period of the nonrelativistic SHO is still given by its natural period even when an external force is present, while the period of the CPO is shifted from its natural value and becomes energy dependent upon application of an external force. The shift in the period can be properly dealt with only when one goes beyond the lowest order in the canonical perturbation theory. The dynamics of the driven CPO is unique in the sense that the lowest-order perturbation theory fails completely and challenges one to go to higher orders or use a more elaborate theory. Here, results of our study based on the second-order perturbation theory are reported.

II. CONSTANT-PERIOD OSCILLATOR

We first present a brief review of the CPO [1]. The CPO is characterized by the unique property that its period of motion is independent of energy in the entire energy range, both nonrelativistic and relativistic. The CPO can thus be considered as a generalized version of the SHO whose period of motion is independent of energy only in the nonrelativistic region.

Mathematically, a constant period means that the action variable I varies linearly with energy, i.e.,

$$I=\frac{1}{2\pi}\oint pdq=\frac{2}{\pi c}\int_0^b\sqrt{[E+mc^2-V(q)]^2-m^2c^4}\,dq$$
$$=\frac{T}{2\pi}E, \tag{1}$$

where $V(q)$, assumed to be symmetric about $q=0$, represents the potential that yields the energy-independent period, b is the amplitude of oscillation at given energy E, and T is the constant period of motion. From Eq. (1), one can obtain, using the technique of Laplace transform,

$$\int_0^\infty e^{-\lambda E}V^{-1}(E)dE=\frac{cT}{4mc^2}\frac{1}{\lambda^2 e^{\lambda mc^2}K_1(\lambda mc^2)}, \tag{2}$$

where K_1 denotes the modified Bessel function of order 1. Equation (2), in principle, allows one to determine V^{-1}, the inverse function of V, and thus $V(q)$. No analytic expression in terms of known functions, however, has been found for the potential $V(q)$.

The behavior of $V(q)$ in the vicinity of $q=0$ is determined by the motion of the CPO in the nonrelativistic limit. By utilizing the asymptotic expansion of K_1 for large λmc^2, one obtains from Eq. (2)

$$V(q)\cong\frac{1}{2}m\left(\frac{2\pi q}{T}\right), \tag{3}$$

which indicates that $V(q)$ approaches the harmonic potential as $q\to 0$. The potential $V(q)$ diverges as q approaches $\pm cT/4$. The behavior of $V(q)$ near $q\cong\pm cT/4$ can be determined by utilizing the power series expansion of K_1 for small λmc^2, and is given by

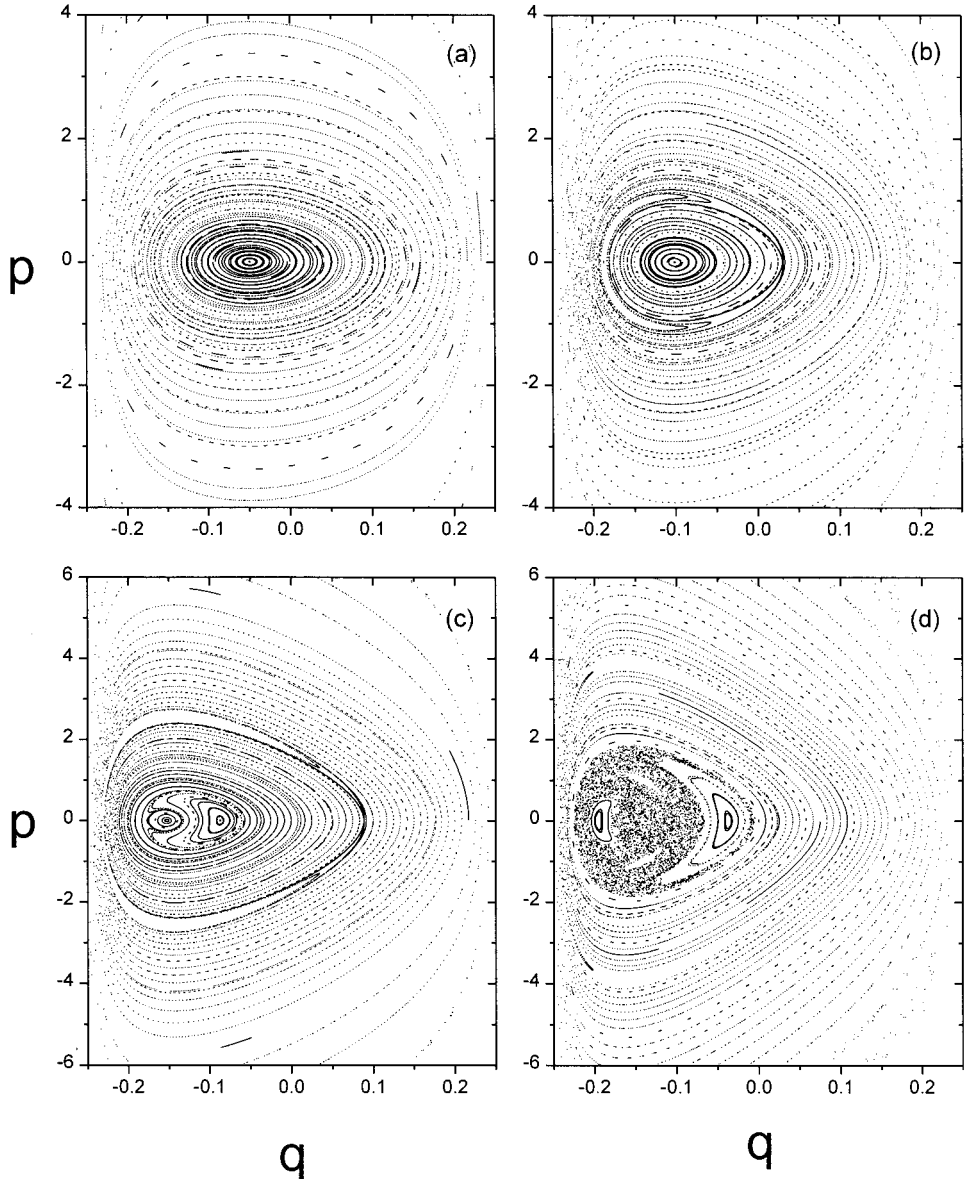

FIG. 1. Poincaré phase-space maps for the driven CPO at (a) $F_0=2$, (b) $F_0=5$, (c) $F_0=9$, and (d) $F_0=13$ (in arbitrary units). The parameters are $m=1$, $c=1$, $w=1$ and $w_0=2\pi$ (in arbitrary units).

$$V(q)\cong mc^2+\frac{mc^2}{\sqrt{2}}\frac{1}{\sqrt{1-4|q|/cT}}. \tag{4}$$

In the immediate vicinity of $q=\pm cT/4$, $V(q)$ is almost a vertical line. This can be understood because, in the ultrarelativistic limit, the velocity of the oscillator is $v\cong c$ and changes little with respect to energy. If the period of oscillation is still to remain independent of energy, the amplitude of oscillation should remain constant regardless of energy, which reguires $V(q)$ to be a vertical line.

Although no exact analytic formula exists for the potential $V(q)$, some approximate formulas were found that closely reproduce the exact potential for the entire range of q, $-cT/4<q<cT/4$. Two examples are given below:

$$V_1(q)=\frac{mc^2\pi^2}{2}\left\{\left[1-\left(\frac{4q}{cT}\right)^2\right]^{-1/4}-1\right\}, \tag{5}$$

$$V_2(q)=\frac{mc^2}{0.3}\left\{\frac{\cosh\left[\frac{1}{20}(2\pi q/cT)^2\right]}{\cos^{0.3}(2\pi q/cT)}-1\right\}. \tag{6}$$

Both Eqs. (5) and (6) satisfy Eq. (3) in the limit $q\to 0$, but neither is consistent with Eq. (4) in the limit $q\to\pm cT/4$. Nevertheless, the two approximate formulas have been found to yield a constant period to within 0.2% of fractional error in both the nonrelativistic and relativistic energy regions. When high accuracy is required, the exact $V(q)$ can be obtained numerically, as described in Ref. [1]. The potential $V(q)$ generally has a bell-shaped curve; it behaves like a harmonic potential in the vicinity of $q=0$, but the slope of the potential curve increases as q moves from zero toward $\pm cT/4$, until it becomes virtually a vertical line at $q=\pm cT/4$.

III. POINCARÉ MAPS

We now consider the CPO driven by a time-periodic force and present in this section results of our numerical computation of Poincaré phase-space maps. The Hamiltonian for the driven CPO is

$$H=\sqrt{p^2c^2+m^2c^4}+V(q)+qF_0\cos wt, \tag{7}$$

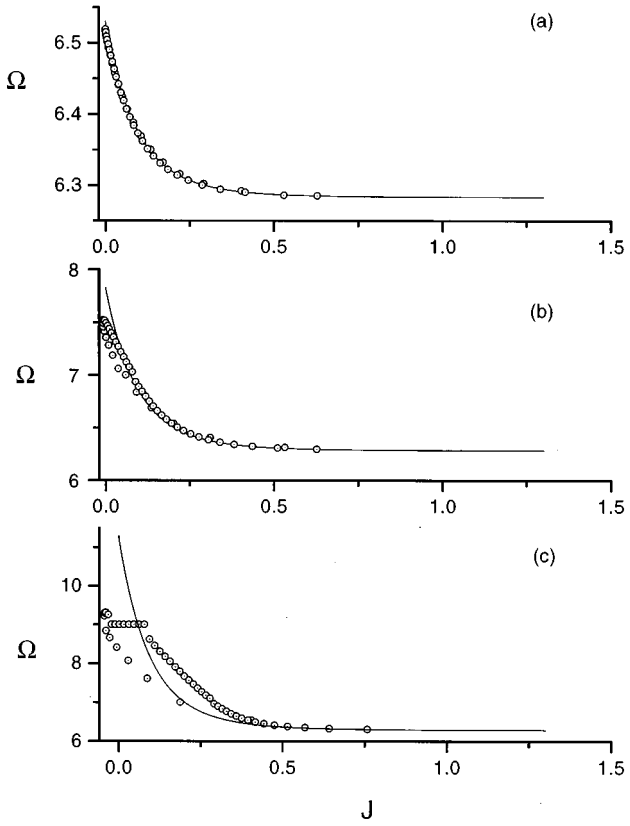

FIG. 2. Frequency of oscillation Ω vs the action variable J obtained theoretically using Eq. (22) (solid curves) and numerically from the Poincaré maps (circles) at (a) $F_0=2$, (b) $F_0=5$, and (c) $F_0=9$ (in arbitrary units). The parameters are $m=1, c=1, w=1$, and $w_0=2\pi$ (in arbitrary units).

where $V(q)$ is the constant period potential described in the previous section. In our numerical computation, both the potential numerically obtained and the approximate analytic expressions of Eqs. (5) and (6) were used and found to give virtually identical maps. $V(q)$ was chosen such that the natural period of the CPO is $T=1$, i.e., the frequency of oscillation in the absence of an external force is $w_0=2\pi$, and m, c, and w were taken to be $m=1$, $c=1$, $w=1$. With w_0 and w as chosen above, the resonance condition

$$\frac{w}{\Omega}=\frac{m}{n}(m,n \text{ integers}) \tag{8}$$

cannot be satisfied, if Ω, the frequency of oscillation in the presence of an external force, is taken to be $\Omega=w_0$, as is usually done in the lowest-order canonical perturbation theory. The phase-space maps shown below, however, indicate clearly the existence of resonances and thus the need for higher-order perturbation theory.

Figure 1 shows Poincaré phase-space maps for our driven CPO obtained through numerical computation. At $F_0=2$, the trajectories are seen to revolve around the central fixed point, a normal behavior one would expect also from, for example, a driven SHO in the nonrelativistic regime. At $F_0=5$, however, a nonlinear resonance appears with the elliptic and hyperbolic fixed points located respectively at $(q=-0.1874,p=0)$ and $(q=0.0307,p=0)$. We see that, at

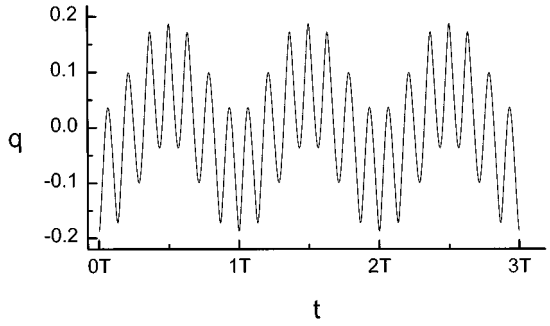

FIG. 3. Trajectory (q vs time) initiated at the elliptic fixed point of the 7:1 resonance. The parameters are $m=1, c=1, w=1$, and $w_0=2\pi$ (in arbitrary units).

$F_0=9$, these fixed points are located further away from the central fixed point and a second resonance with the elliptic and hyperbolic fixed points at $(q=-0.0870,p=0)$ and $(q=-0.1772,p=0)$ is generated. Finally, at $F_0=13$, a considerable portion of the phase space is occupied by a chaotic sea.

IV. RESONANCE ANALYSIS

In this section we analyze the motion of the driven CPO using the second-order perturbation theory. In order to apply the canonical perturbtion theory, it is convenient first to go to the action-angle space. The Hamiltonian is written in terms of the action-angle variables I, θ as

$$H=w_0 I+\epsilon F_0\sum_n A_n(I)\cos n\theta\ \cos wt, \tag{9}$$

where the parameter ϵ is introduced to identify the driving force term as the perturbation and will be set $\epsilon=1$ at the end of the calculation, and $A_n(I)$'s are defined as

$$q=\sum_n A_n(I)\cos n\theta. \tag{10}$$

$A_n(I)$'s vanish for even n if the potential is symmetric, and approach the SHO limit

$$A_n(I)=\sqrt{\frac{2I}{mw_0}}\delta_{n1} \tag{11}$$

TABLE I. The location (q value) of the fixed points of the resonances obtained theoretically from the second-order perturbation theory and numerically from the Poincaré maps. For all fixed points listed, $p=0$. The parameters are $m=1, c=1, w=1$, and $w_0=2\pi$ (in arbitrary units).

		Theoretical		Numerical	
F_0	$\Omega:w$	Elliptic	Hyperbolic	Elliptic	Hyperbolic
4	7:1	−0.16	−0.01	−0.14	−0.02
5	7:1	−0.19	0.02	−0.19	0.03
6	7:1	−0.21	0.03	−0.21	0.06
9	7:1	−0.23	0.02	−0.23	0.09
9	9:1	−0.07	−0.22	−0.09	−0.18

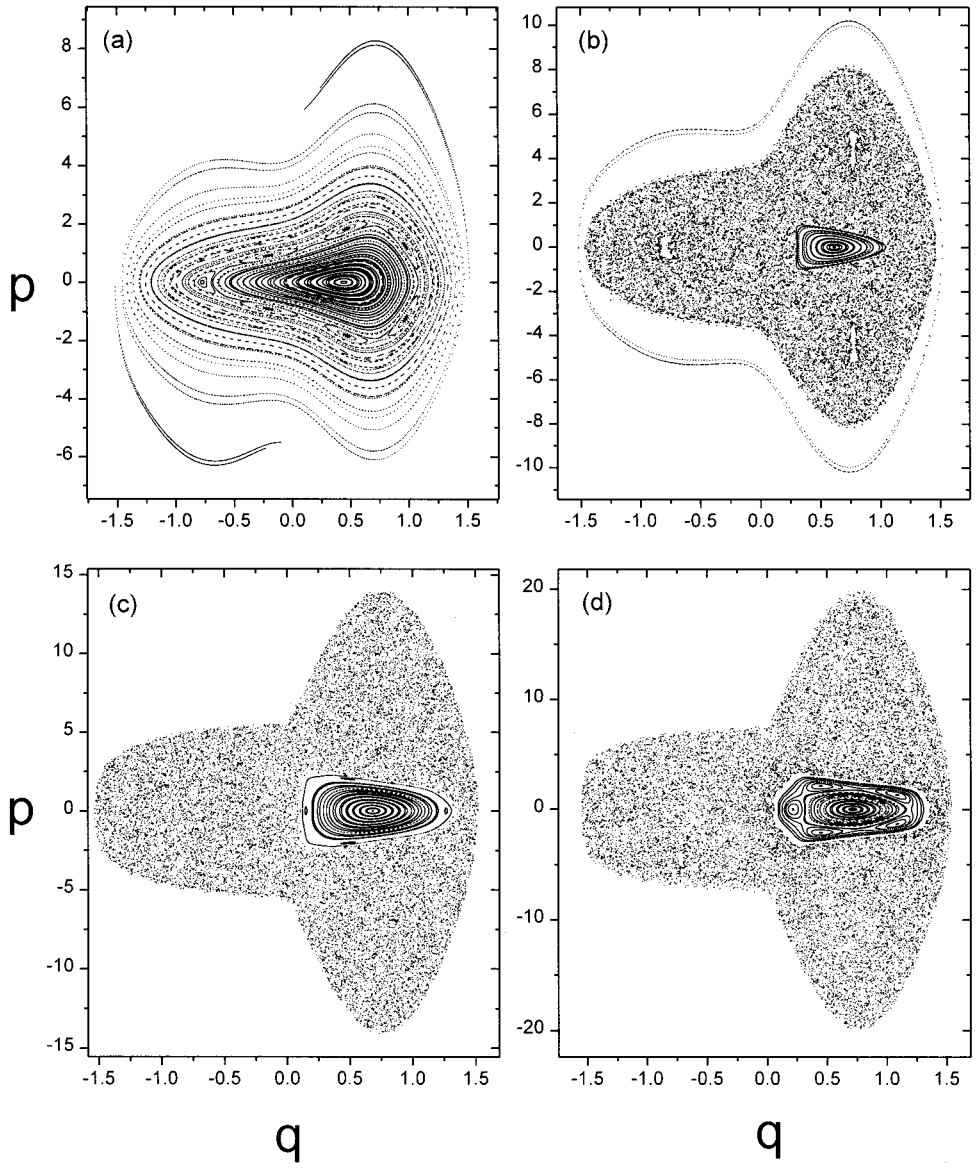

FIG. 4. Poincaré phase-space maps for the driven CPO at (a) $F_0=2$, (b) $F_0=5$, (c) $F_0=9$, and (d) $F_0=13$ (in arbitrary units). The parameters are $m=1, c=1$, $w=2$, and $w_0=1$ (in arbitrary units).

when the oscillator energy is sufficiently nonrelativistic that $w_0 I \ll mc^2$. In general for the CPO, $A_n(I)$'s cannot be expressed in an analytic form but were obtained numerically in Ref. [1] for $n=1-11$. $A_n(I)$'s usually decrease fast as n is increased, and it is often sufficient to consider only the first few.

In the canonical perturbation theory [3], one seeks a canonical transformation from the action-angle variables (I,θ) to a new set of action-angle variables (J,ϕ), which allows an identification of the action variable J as an invariant to a desired order of perturbation. The generating function for the desired transformation is written as

$$S(J,\theta,t)=J\theta+\epsilon S(J,\theta,t)+\epsilon^2 S_2(J,\theta,t)+\cdots. \quad (12)$$

The relation between I,θ and J,ϕ is given by

$$I=\frac{\partial S}{\partial\theta}=J+\epsilon\frac{\partial S_1(J,\theta,t)}{\partial\theta}+\epsilon^2\frac{\partial S_2(J,\theta,t)}{\partial\theta}+\cdots, \quad (13)$$

$$\phi=\frac{\partial S}{\partial J}=\theta+\epsilon\frac{\partial S_1(J,\theta,t)}{\partial J}+\epsilon^2\frac{\partial S_2(J,\theta,t)}{\partial J}+\cdots, \quad (14)$$

and the new Hamiltonian by

$$K(J,\phi,t)=H(I,\theta,t)+\frac{\partial S}{\partial t}. \quad (15)$$

Substituting Eqs. (9) and (12) into Eq. (15) and utilizing Eqs. (13) and (14) to collect terms of the same order in ϵ, we obtain

$$K(J,\phi,t)=w_0 J+\epsilon\left[w_0\frac{\partial S_1}{\partial\theta}+\frac{\partial S_1}{\partial t}+F_0\sum_n A_n(J)\cos n\theta\,\cos wt\right]+\epsilon^2\left[w_0\frac{\partial S_2}{\partial\theta}+\frac{\partial S_2}{\partial t}+F_0\sum_n\frac{dA_n(J)}{dJ}\frac{\partial S_1}{\partial\theta}\cos n\theta\,\cos wt\right]+\cdots. \quad (16)$$

Now, S_1 and S_2 are to be chosen so as to eliminate the θ- and t-dependent parts in the brackets of Eq. (16). Straightforward algebraic manipulation yields

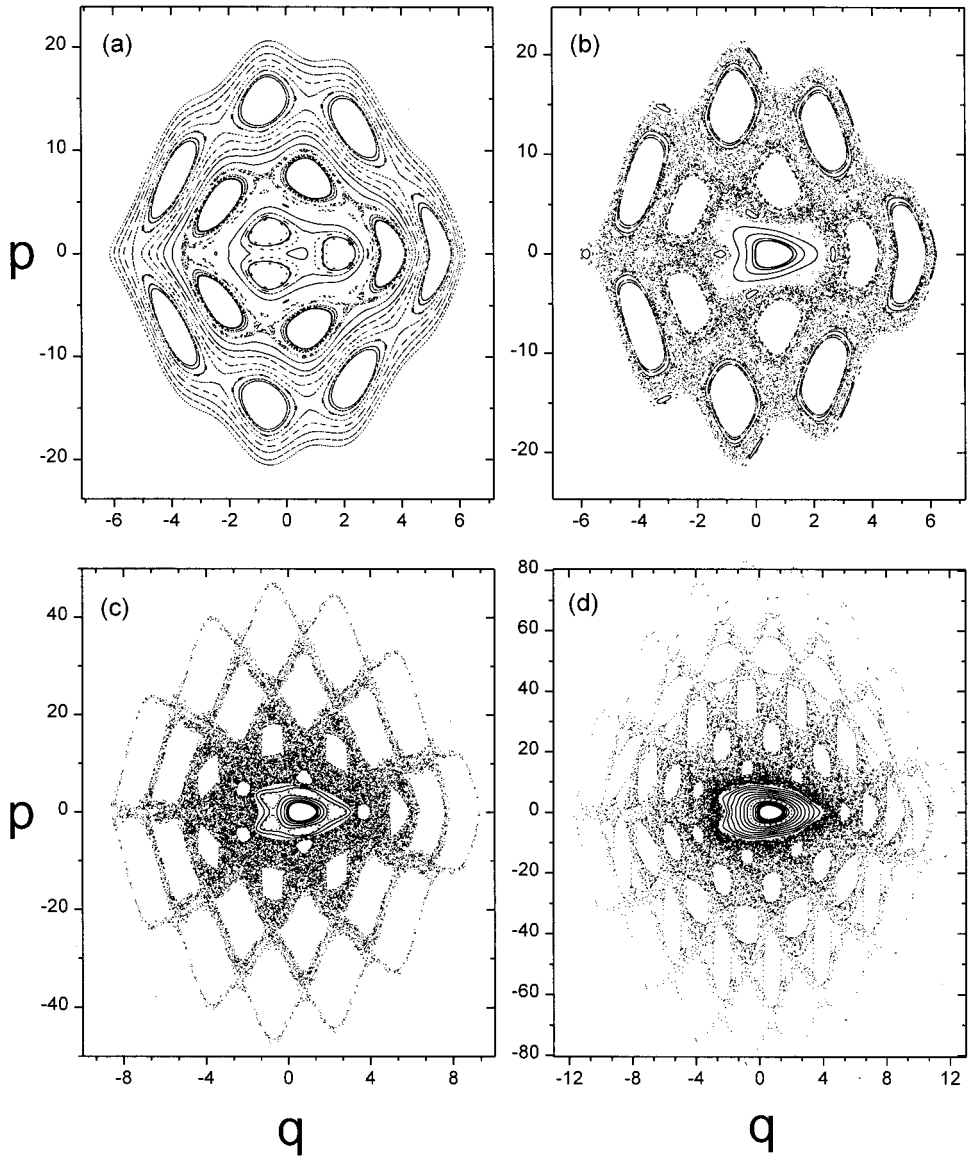

FIG. 5. Poincaré phase-space maps for the driven SHO at (a) $F_0=2$, (b) $F_0=5$, (c) $F_0=9$, and (d) $F_0=13$ (in arbitrary units). The parameters are $m=1$, $c=1$, $w=2$, and w_0 (natural frequency in the nonrelativistic limit) $=1$ (in arbitrary units).

$$S_1(J,\theta,t)=-\frac{F_0}{2}\sum_n A_n(J)\left[\frac{\sin(n\theta+wt)}{nw_0+w}+\frac{\sin(n\theta-wt)}{nw_0-w}\right], \tag{17}$$

and a somewhat more complex expression for S_2. Equation (16) then becomes

$$K(J,\phi,t)=w_0J+\epsilon K_1(J)+\epsilon^2K_2(J)+\epsilon^3K_3(J,\phi,t)+\cdots, \tag{18}$$

where

$$K_1(J)=\left\langle F_0\sum_n A_n(J)\cos n\theta\cos wt\right\rangle=0, \tag{19}$$

$$K_2(J)=\left\langle F_0\sum_n \frac{dA_n(J)}{dJ}\frac{\partial S_1}{\partial\theta}\cos n\ \theta\cos wt\right\rangle$$
$$=-\frac{F_0^2}{8}\sum_n \frac{d[A_n(J)]^2}{dJ}\frac{n^2w_0}{(nw_0+w)(nw_0-w)}. \tag{20}$$

Here, the bracket $\langle\ \rangle$ denotes a quantity averaged over θ and t; i.e.,

$$\langle f(J,\theta,t)\rangle=\frac{1}{T}\int_0^T dt\frac{1}{2\pi}\int_0^{2\pi}d\theta f(J,\theta,t). \tag{21}$$

The frequency of oscillation in the presence of the external force is given, to second order of perturbation, by

$$\Omega(J)=\frac{\partial K}{\partial J}=w_0-\frac{F_0^2}{8}\sum_n \frac{d^2[A_n(J)]^2}{dJ^2}\frac{n^2w_0}{(nw_0+w)(nw_0-w)}, \tag{22}$$

where we set $\epsilon=1$.

Equation (22) indicates that the frequency of the CPO becomes energy dependent when an external force is present. Substituting Eq. (22) into Eq. (8), one can now determine whether and where the $n:m$ resonance corresponding to $\Omega:w=n:m$ exists. In Fig. 2 we show $\Omega(J)$ as a function of J at different values of F_0 obtained theoretically using Eq. (22) with $A_n(J)$ determined numerically as well as numerically from the Poincaré maps. It is seen that the second-order

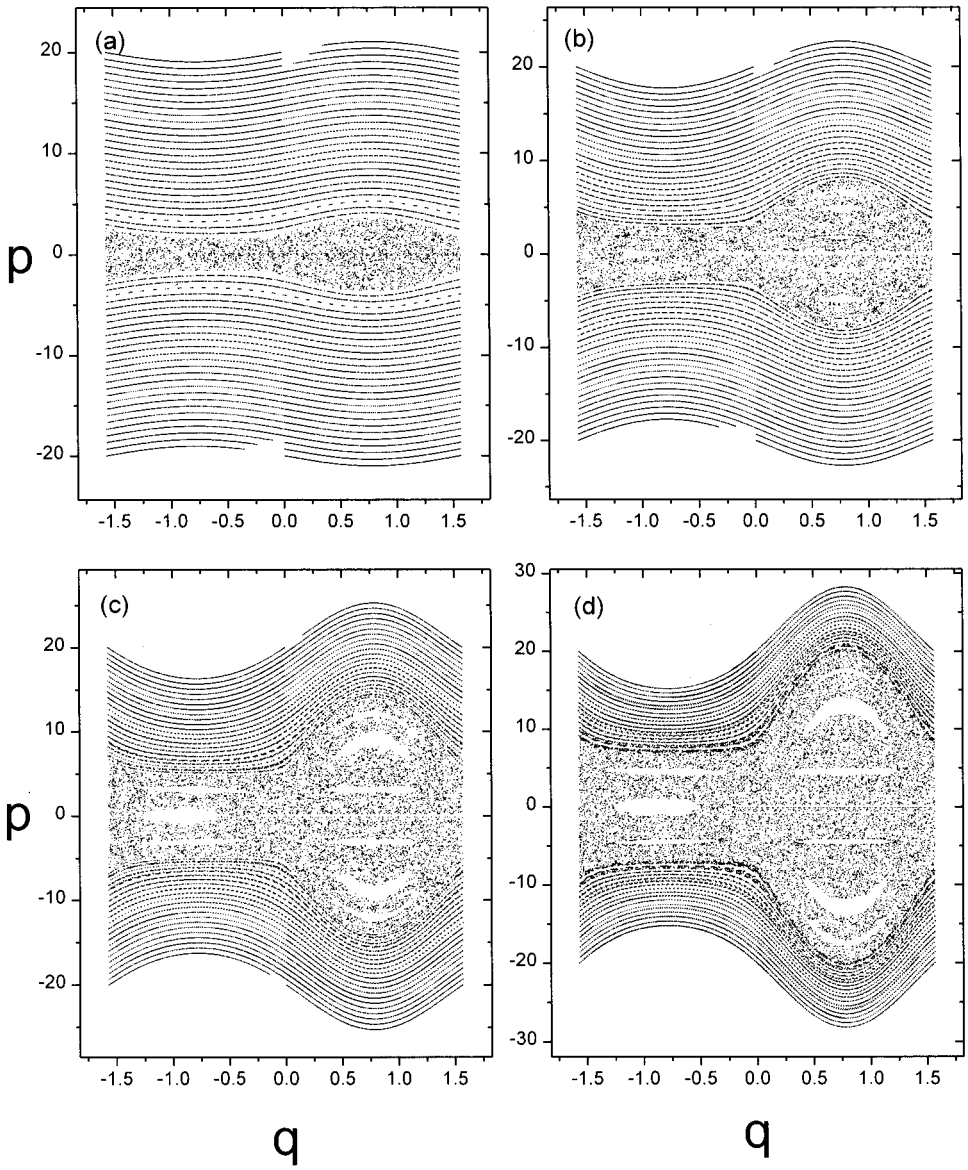

FIG. 6. Poincaré phase-space maps for the driven square-well oscillator at (a) $F_0=2$, (b) $F_0=5$, (c) $F_0=9$, and (d) $F_0=13$ (in arbitrary units). The parameters are $m=1$, $c=1$, $w=2$, and w_0 (natural frequency in the ultrarelativistic limit) $=1$ (in arbitrary units).

perturbation theory on which Eq. (22) is based yields values of Ω in good agreement with the exact numerical values. We note, in particular, that the maximum value of Ω is greater than 7 at $F_0=5$ but less than 7 at $F_0=2$. The resonance condition, Eq. (8), can thus be satisfied with $m=1$ and $n=7$ at $F_0=5$, but not at $F_0=2$. This suggests that the resonance that appears at $F_0=5$ but is missing at $F_0=2$, as observed from Fig. 1, is the 7:1 resonance. That this is indeed the case is confirmed by our numerical calculation of the trajectory initiated at the elliptic fixed point $(q=-0.1874, p=0)$ of the resonance shown in Fig. 3. We observe also from Fig. 2 that the maximum value of Ω is greater than 9 at $F_0=9$, indicating that the second resonance seen in Fig. 1(c) is the 9:1 resonance.

The location of each fixed point of the resonances can be approximately determined by straightforward algebra. For a given value of F_0, we first solve Eq. (22) to obtain the value of J that yields Ω corresponding to the resonance being considered, say $\Omega=7$ if a fixed point of the 7:1 resonance is to be determined. We then use the relation of Eq. (13) to determine I corresponding to the fixed point from this value of J, taking $t=2\pi n/w$ and assigning an appropriate value of θ. For the elliptic or hyperbolic fixed point of the 7:1 or 9:1 resonance of Fig. 1(c), the appropriate value of θ is 0 or π, which corresponds to $p=0$. With I and θ determined as above, q can be obtained from Eq. (10). The locations of the fixed points evaluated as above are shown in Table I along with those determined numerically from the phase-space plots. The agreement between the two sets is seen to be reasonably good, which gives an added confirmation that the second-order perturbation theory provides a reasonably accurate description of the dynamics of the CPO being considered.

V. COMPARISON WITH SIMPLE HARMONIC OSCILLATOR AND SQUARE-WELL OSCILLATOR

Further physical insights into the dynamics of the driven CPO can be gained by comparing the behavior of the driven CPO with that of the driven SHO and the driven square-well oscillator. For that purpose we present in Figs. 4–6 Poincaré phase-space maps for relativistic oscillators in the constant period potential, harmonic potential, and square-well potential, respectively. For convenience of comparison, we have

chosen the driving frequency $w=2$ and the natural frequency of each oscillator $w_0=1$ while $m=1$ and $c=1$ as before. Here the natural frequency of the SHO is defined as that in the nonrelativistic limit ($v \ll c$), while the natural frequency of the oscillator in the square-well potential is defined as that in the ultrarelativistic limit ($v \cong c$). Thus, $w_0=1$ for the square well means that the half width of the well is $a=\pi/2$. Comparing Figs. 4–6, we first note that the square-well motion is most easily chaotic. This is because the low-energy region of the square-well potential is occupied densely with high-period resonances that overlap easily upon application of even a weak external force. At relatively high values of F_0, the phase-space maps of the square well and CPO resemble each other, which reflects the fact that the CPO in the ultrarelativistic limit behaves like a particle in a square well. The SHO's phase-space map compared with that of the CPO is characterized by many primary resonances that show up clearly in the map. We should note, however, that the size of the chaotic sea is smaller for the CPO than for the SHO. For example, at $F_0=13$, the chaotic sea spreads over the region between $p \cong -20$ and $p \cong 20$ for the CPO, while for the SHO the range of p spanned by the chaotic sea is three times as large. This results from the fact that the CPO with its energy-independent period in the absence of an external force is more strongly resistant to generation of nonlinear resonances than the SHO when an external force is applied.

VI. DISCUSSION

A sufficient condition for nonlinear resonances to be generated and consequently for chaos to be exhibited by an oscillator is that the oscillation frequency varies with energy. Although the CPO has an energy-independent frequency (or period) of motion in the absence of an external force, its frequency is shifted and becomes energy dependent when an external force is applied. One can thus understand that the CPO can behave chaotically when it is driven by a sufficiently strong force. One may wonder whether the oscillation frequency is shifted from its natural value also for the case of a nonrelativistic simple harmonic oscillator when an external force is present. That, however, is not the case. One can in fact easily show that, by substituting Eq. (11) into Eq. (22), $\Omega=w_0$, i.e., the frequency of the SHO in the presence of an external force is identical to that in the absence of an external force. The nonrelativistic SHO seems unique in this respect. All other systems including the CPO suffer a shift in the oscillation frequency when an external force is applied. The analogy between the CPO and the nonrelativistic SHO does not go much beyond that they both have a constant frequency of motion in the absence of an external force. It has already been found that quantum energy eigenvalues of the CPO are not equally spaced [1].

Throughout this paper we have implicitly assumed that the external force may vary in time but is independent of spatial coordinates. Although an analysis similar to the one described in Sec. IV can still be applied to the case when an external force varies both in time and space, some new effects appear. It can be shown, for example, that even the frequency of the nonrelativistic SHO becomes energy dependent in the presence of a space-time varying external force [4]. Consequently, nonlinear resonances can be generated and when they overlap, chaos can be exhibited by a nonrelativistic SHO driven by a space-time varying force. This is of some practical importance in plasma physics, because the cyclotron motion of a charged particle interacting with an electromagnetic wave can be described by a simple harmonic oscillator driven by an external force that varies periodically both in time and in space [5–8]. We expect that the second-order canonical perturbation theory described in this paper can also be used to describe the resonances and chaos occurring in such motion. Details will be described elsewhere.

ACKNOWLEDGMENTS

This research was supported in part by the Ministry of Science and Technology of Korea (MOST) under the project ''High-Performance Computing-Computational Science and Engineering (HPC-COSE),'' by the Agency for Defense Development (ADD) of Korea, and by the Korea Science and Engineering Foundation (KOSEF) under Grant No. 961-0202-011-2.

[1] J. H. Kim, S. W. Lee, H. Maassen, and H. W. Lee, Phys. Rev. A **53**, 2991 (1996).
[2] J. H. Kim and H. W. Lee, Phys. Rev. E **51**, 1579 (1995).
[3] A. J. Lichtenberg and M. A. Lieberman, *Regular and Stochastic Motion* (Springer-Verlag, New York, 1983).
[4] S. W. Lee and H. W. Lee, Phys. Rev. E (to be published).
[5] G. M. Zaslavsly, R. Z. Sagdeev, D. A. Usikov, and A. A. Chernikov, *Weak Chaos and Quasi-regular Patterns* (Cambridge University Press, Cambridge, 1991).
[6] A. Fukuyama, H. Momota, R. Itatani, and T. Takizuka, Phys. Rev. Lett. **38**, 701 (1977).
[7] C. F. F. Karney, Phys. Fluids **21**, 1584 (1978).
[8] G. M. Zaslavsky, M. Y. Zakharov, R. Z. Sagdeev, D. A. Usikov, and A. A. Chernikov, Zh. Éksp. Teor. Fiz. **91**, 500 (1986) [Sov. Phys. JETP **64**, 294 (1986)].